Environmental Science and Pollution Research (2024) 31:3526–3544
https://doi.org/10.1007/s11356-023-31414-7

RESEARCH ARTICLE

Detection of atmospheric aerosols and terrestrial nanoparticles collected in a populous city in southern Brazil

Marluse Guedes Bortoluzzi[1] · Alcindo Neckel[1,2] · Brian William Bodah[3,4] · Grace Tibério Cardoso[1] · Marcos L. S. Oliveira[5,6] · Paloma Carollo Toscan[2] · Laércio Stolfo Maculan[1] · Liliana P. Lozano[5,7] · Eliane Thaines Bodah[3,8] · Luis F. O. Silva[5,7,9]

Received: 11 September 2023 / Accepted: 4 December 2023 / Published online: 12 December 2023

Abstract

The main objective of this study is to analyze hazardous elements in nanoparticles (NPs) (smaller than 100 nm) and ultrafine particles (smaller than 1 μm) in Porto Alegre City, southern Brazil using a self-made passive sampler and Sentinel-3B SYN satellite images in 32 collection points. The Aerosol Optical Thickness proportion (T550) identification was conducted using images of the Sentinel-3B SYN satellite at 634 points sampled in 2019, 2020, 2021, and 2022. Focused ion beam scanning electron microscopy analyses were performed to identify chemical elements present in NPs and ultrafine particles, followed by single-stage cascade impactor to be processed by high-resolution transmission electron microscopy. This process was coupled with energy-dispersive X-ray spectroscopy and later analysis via secondary ion mass spectrometry. Data was acquired from Sentinel-3B SYN images, normalized to a standard mean of 0.83 μg/mg, at moderate spatial resolution (260 m), and modeled in the Sentinel Application Platform (SNAP) software v.8.0. Statistical matrix data was generated in the JASP software (Jeffreys's Amazing Statistics Program) v.0.14.1.0 followed by a K-means cluster analysis. The results demonstrate the presence of between 1 and 100 nm particles of the following chemical elements: Si, Al, K, Mg, P, and Ti. Many people go through these areas daily and may inhale or absorb these elements that can harm human health. In the Sentinel-3B SYN satellite images, the sum of squares in cluster 6 is 168,265 and in cluster 7 a total of 21,583. The use of images from the Sentinel-3B SYN satellite to obtain T550 levels is of great importance as it reveals that atmospheric pollution can move through air currents contaminating large areas on a global scale.

Keywords Nanoparticles · Ultrafine particulates · Atmospheric aerosols · Future projects · Global scale

Responsible Editor: Gerhard Lammel

✉ Alcindo Neckel
alcindo.neckel@atitus.edu.br

[1] Atitus Educação, 304 – Villa Rodrigues, Passo Fundo, RS 99070-220, Brazil

[2] University of Minho, UMINHO, 4710-057 Porto, Portugal

[3] Thaines and Bodah Center for Education and Development, 840 South Meadowlark Lane, Othello, WA 99344, USA

[4] Workforce Education & Applied Baccalaureate Programs, Yakima Valley College, South 16th Avenue & Nob Hill Boulevard, Yakima, WA 98902, USA

[5] Department of Civil and Environmental Engineering, Universidad de La Costa, CUC, Calle 58 # 55–66, Barranquilla, Atlántico, Colombia

[6] Santa Catarina Research and Innovation Support Foundation (Fapesc), Florianópolis, SC 88030-902, Brazil

[7] Postgraduate Doctoral Program in Society, Nature and Development, Universidade Federal Do Oeste Do Pará, UFOPA, Paraná 68040-255, Brazil

[8] State University of New York, Onondaga Community College, 4585West Seneca Turnpike, Syracuse, NY 13215, USA

[9] CDLAC – Data Collection Laboratory and Scientific Analysis LTDA, Nova Santa Rita 92480-000, Brazil

Introduction

Air pollution by the concentration of hazardous elements suspended in the atmosphere in volumetric proportions of nanoparticles (NPs) and ultrafine particles is negatively impacting the natural environment and posing a threat to human health (Saikia et al. 2017; Vithanage et al. 2022; Neckel et al. 2023). Atmospheric pollution is the result of gases being releases into the atmosphere as particles of chemical elements that impact the environment and can cause health problems mainly in large cities (Che et al. 2022; Xu et al. 2023). Gases in high concentrations in the atmosphere such as ammonia (NH_3), chlorofluorocarbons (CFCs), volatile organic compounds (VOCs), carbon dioxide (CO_2), carbon monoxide (CO), sulfur oxides (SO_x), and nitrogen oxides (NO_x) can aggregate particulate matter that forms NPs and ultrafine particles (Ballikaya et al. 2022; Vouitsis et al. 2023). Due to their lower density, these NPs and ultrafine particles can remain in the atmosphere for a long period with the capability of contaminating large regions, depending on the intensity of the displacement of the air masses responsible (Peng et al. 2023).

After displacement, the NPs and ultrafine particles present in the atmosphere are allocated on the surface of building and environment. This causes accumulation of suspended particles that include elements of different chemical characteristics that affect health of residents, passengers, and pedestrians (Trejos et al. 2021; Vouitsis et al. 2023). According to Pryshchepa and Buszewski (2020), Martinello et al. (2022), Silva et al. (2022), and Neckel et al. (2023), studies aimed at identifying toxic elements present in NPs and ultrafine particles using advanced equipment such as the FIB-SEM and HR-HE HAS are very important. These studies are structured as follows: (1) Pryshchepa and Buszewski (2020) emphasized that silver NPs' investigation techniques need more efforts on a global scale. NPs and atmospheric ultrafine particles can cause damage irreversible due to the high amount of toxic salts involving these particulates (Pryshchepa and Buszewski 2020); (2) Martinello et al. (2022) studied NPs and ultrafine atmospheric particles generated by artisanal ceramic factories in Brazil that used wood combustion. They identified NPs and ultrafine particles (< 10 nm) containing high proportions of the toxic elements arsenic (As), cadmium (Cd), mercury (Hg), and lead (Pb); (3) Silva et al. (2022) analyzed air pollution in North Africa and detected particles from medieval historic architecture, containing chemical elements such as aluminum (Al), potassium (K), silicon (Si), and magnesium (Mg). These particles were considered harmful to the quality of historic buildings listed by the United Nations Educational, Scientific and Cultural Organization (UNESCO), in addition to presenting risks of contamination by these dangerous elements for human health; (4) Neckel et al. (2023) evaluated air pollution in the city of Budapest (Central Europe), via passive samplers aimed at identifying hazardous chemical elements present in NPs and ultrafine particles, in addition to the use of Sentinel-3B SYN satellite images for the identification of aerosols atmospherics at T550. The presence of NPs and ultrafine particles containing toxic elements such as arsenic, chromium, lead, mercury, nickel, titanium, and vanadium was noticed (Neckel et al. 2023).

Terrestrial studies by SMPS (Pryshchepa and Buszewski 2020; Martinello et al. 2022; Silva et al. 2022; Neckel et al. 2023) with integrated studies using satellite images for geospatial data collection make possible to obtain more robust analyses of the environment, in regard to the quantitative variations of atmospheric aerosols (Zoheir et al. 2019; Neckel et al. 2023). The use of the Sentinel-3B SYN satellite means has undergone geospatial tests by the European Space Agency—ESA (2023a, 2023b, 2023c), and it is one of the most current and reliable tools for aerosols quantitative analysis by T550 (Zhu et al. 2022; Sánchez-Zapero et al. 2023).

The main goal of this study is to analyze the hazardous elements as nanoparticles (NPs) and ultrafine particles present in 32 points sampled in the city of Porto Alegre, Brazil. In addition to the identification of Aerosol Optical Thickness proportion (T550) by images of the Sentinel-3B SYN satellite at 634 points sampled in the years 2019, 2020, 2021, and 2022. This study enhances the terrestrial analysis approaches of NPs and ultrafine particles collected by SMPS, adding to the use of Sentinel-3B SYN. The ESA through the European Union's Earth Observation Program (Copernicus) supports atmospheric research and provides a high degree of sampling reliability to identify the number of aerosols per T550.

Material and methods

Study area

Porto Alegre City is located in a Metropolitan Region in the state of Rio Grande do Sul, Southern Brazil (Fig. 1). It has a territorial area of 495,390 km^2, totaling 1,492,530 inhabitants, and a demographic density of 3012 inhabitants/km^2 (IBGE 2023). The predominant climate in Porto Alegre is subtropical or humid subtropical, where there are distinct four seasons (autumn: March to June; winter: July to September; spring: September to December; and summer: December to March). Sharp peaks in temperatures occur in the summer and winter seasons (INPE 2022). Porto Alegre has the highest temperatures in January (summer) corresponding to 30 °C, and the lowest temperatures in July (winter) of 10 °C (INPE 2022). The month of September has the

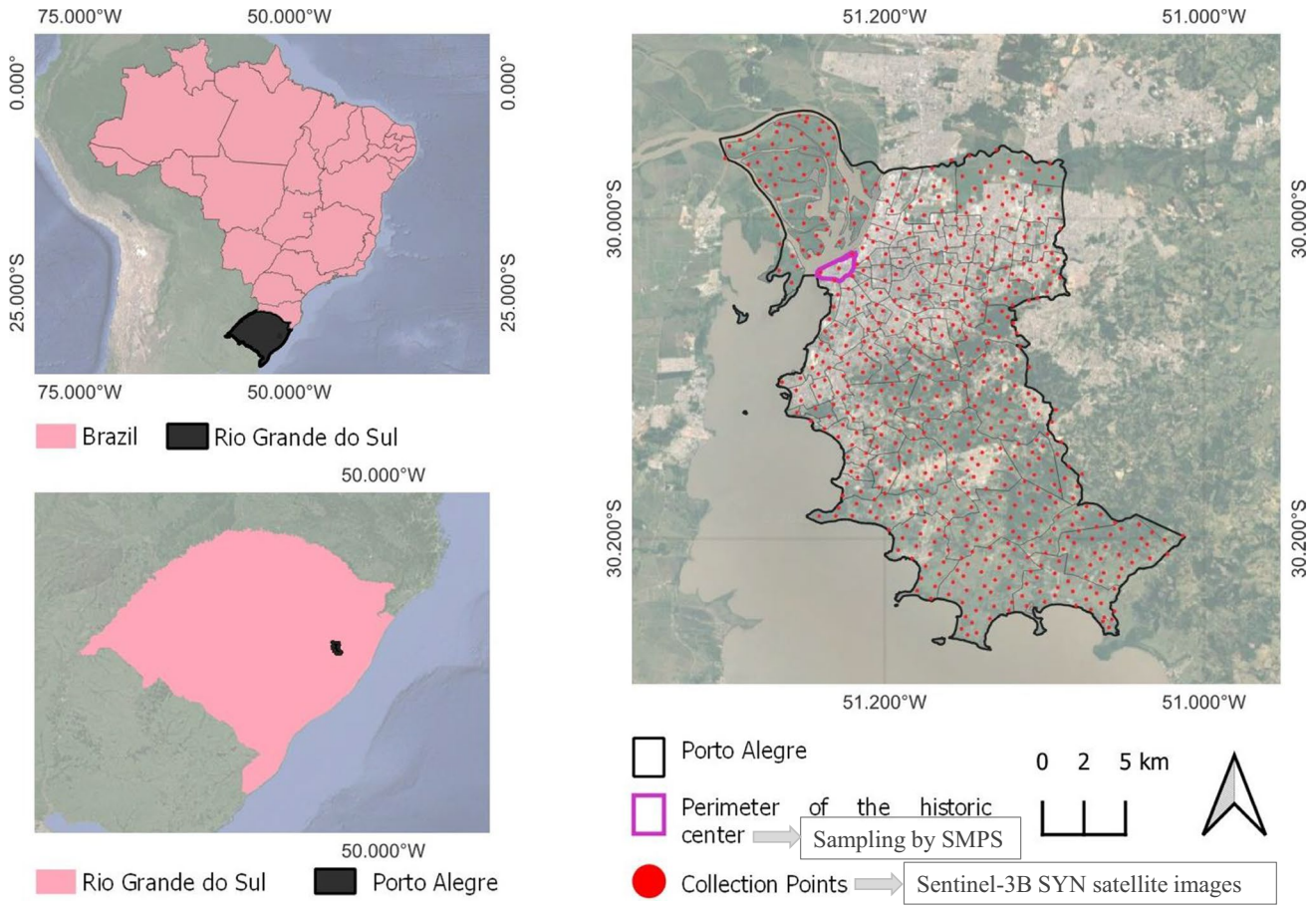

Fig. 1 Location of the city of Porto Alegre (capital of the state of Rio Grande do Sul, Brazil) in relation to the SMPS sampling points utilized in the city's Historical Center neighborhood in conjunction with Sentinel-3B SYN satellite images

highest average precipitation of 136.8 mm, while March has the lowest average precipitation of 84.1 mm (INMET 2023).

There are wind speed variations between 5 and 10 km/h (1.4 and 2.8 m/s), on an average of 2.1 m/s, with more frequent winds coming from the north for 2.3 months (May 22 to July 31), according to the NOAA Air Resources Laboratory (ARL 2023). A maximum of 33% of winds was recorded on June 30, in addition to more frequent winds coming from the east, during the average period of 9.9 months (July 28 to May 24). A maximum average of 54% was recorded on January 1 (INPE 2022; Zorzi et al. 2022; INMET 2023). The city has 1708 factories and an average flow of 825,000 vehicles (IBGE 2023) responsible for constant emissions of nitrogen oxides, carbon monoxide, and ozone to the atmosphere. These gases impact air quality in part due to meteorological and constrictive conditions, favoring the dispersion of these atmospheric pollutants to other regions, increasing risks to human health (Borrego et al. 2010; Marmett et al. 2021; Abdillah and Wang 2023). Kumar et al. (2016), Rohra et al. (2022), and Neckel et al. (2023) emphasized the need to apply methodologies in studies aimed at identifying air pollutants, usually suspended in the form of nanoparticles and ultrafine particles. Analysis techniques using satellite images along with terrestrial data collected in the field of particulate matter need to take place.

Figure 1 shows the limits of the analyzed area encompassing sampling sites by the self-made passive sampler (SMPS) and by Sentinel-3B SYN satellite images. Oliveira et al. (2021) and Neckel et al. (2023) emphasize the need for this list of techniques, obtained with field collections by SMPS in order to obtain quantitative results of nanoparticles and ultrafine particles present in particles suspended in the atmosphere. In addition, the use of satellite images Sentinel-3B SYN is capable of mediating the proportion of atmospheric aerosols to achieve more robust and realistic quantitative analyses on terrestrial identification of the types of particulate chemical elements found in the origin of these atmospheric aerosols in Porto Alegre, Brazil, and can serve as a methodological model for the development of other studies on a global scale.

Data collection and analytical methods

The first sampling of material suspended in the atmosphere at 32 specific points in the central urban area of Porto Alegre, Brazil took place between April 2 and August 15, 2019. Samplers were spaced between 50 and 80 m and located in areas with greater flow of people and motor vehicles, as referenced in similar collection of particulate matter studies (Zhao et al. 2017; Akhbarizadeh et al. 2021; Aarzoo et al. 2022). These collection points also remained permanent during April 2nd and August 15th of 2020, 2021, and 2022. The collections during the years 2019, 2020, 2021, and 2022 were carried out using SMPS, constructed with polyvinyl chloride (PVC) material (Fig. 2), to avoid entrance of rainwater in the internal part of the SMPS recommended by Herrera and Videla (2009), Morillas et al. (2019), and Neckel et al. (2023).

As a passive sampler, the SMPS collects everything that touches it without any interference (Oliveira et al. 2021; Neckel et al. 2023), demonstrating a greater reliability and preservation of the material sampled in this study. The SMPS was modeled and built based on studies by Oliveira et al. (2021) and Neckel et al. (2023). PVC measuring 50 mm was used, with an external diameter of 50.7 mm and a wall thickness of 1.6 mm. A small piece of foam was attached to the internal environment of the PVC, allowing for the accumulation of nanoparticles (smaller than 100 nm) and ultrafine particles (smaller than 1 µm) within and on the foam. The small size of these particles, many of which contain chemical elements, enables them to remain suspended in the atmosphere for a long period of time. They entered the SMPS through an opening in the PVC (Fig. 2). Oliveira et al. (2021) and Neckel et al. (2023), in their studies in dense urban environments, found that the use of SMPS was efficient in collecting nanoparticles and ultrafine particles on and within the foam inside the sampler. This foam was later sent to the laboratory for quantification of the chemical elements present in the material collected. Foam pieces were replaced every 3 months.

The SMPS were fixed on electric lighting poles, at a height of 1.5 m from the planimetric level of the sidewalk (Fig. 2). This adjustment was a human scale height justified by Xu et al. (2017), Oliveira et al. (2021), and Zou and Yang (2022), as it consists of the average height of human breathing, where aerosols can be inhaled by the respiratory system in the form of NPs and ultrafine particles that are harmful to human health.

Samples of particulate matter were placed in sterilized glass containers and stored in sealed Styrofoam boxes, in order to avoid external contamination. Subsequently, the samples were sent within a period of 24 h to the appropriate laboratories for carrying out the analytical procedures, aiming to identify toxic elements present in the sampled material (Oliveira et al. 2021; Neckel et al. 2023). Sampling was carried out in April and August of the years 2019, 2020, 2021, and 2022; therefore, at the end of this study, 256 samples physical samples were collected. After collection, samples were homogenized and divided into three specimens

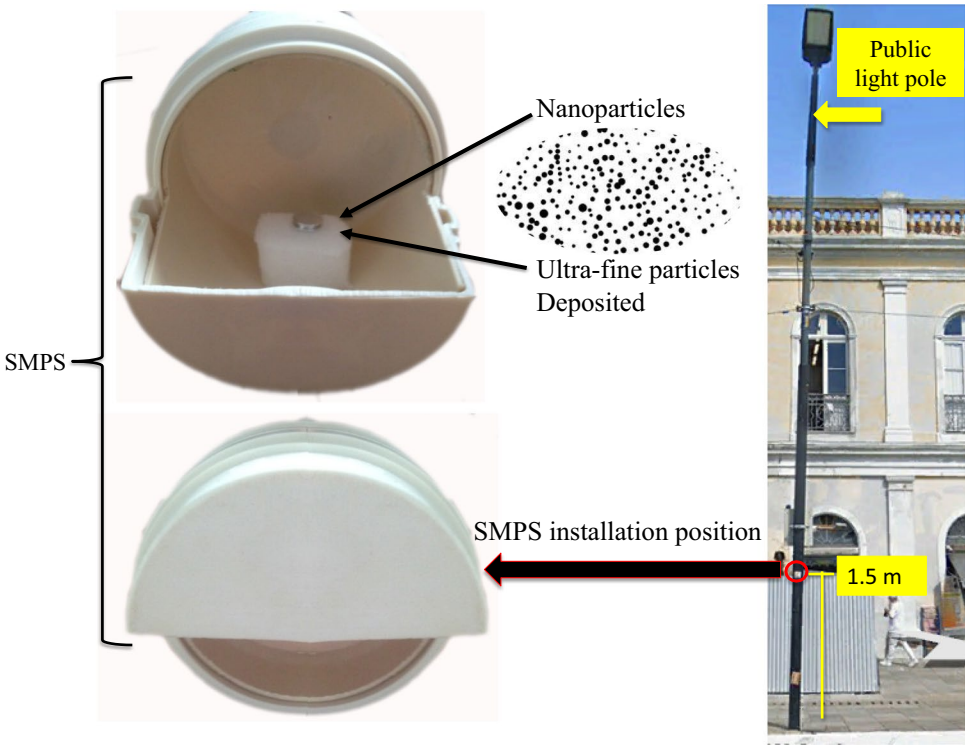

Fig. 2 Self-made passive sampler (SMPS) made from polyvinyl chloride (PVC) material and foam to capture particles suspended in the atmosphere, attached to a public lighting pole at a height of 1.5 m in relation to the planimetric level of the sidewalk, downtown history of the capital Porto Alegre

(3 replicates (K3)), with an average weight per sample unit of 3.2 g. One sample was analyzed immediately as security measure. According to Oliveira et al. (2021) and Neckel et al. (2023), it is necessary to prepare replicated samples.

After homogenization in each annual collection period, the material was studied using advanced electronic microscopy techniques, where it was possible to evaluate both NPs and proportions greater than 10 µm, by focused ion beam scanning electron microscopy (FIB-SEM) for the identification of chemical elements (Jia et al. 2020; Yuan et al. 2021). Then, samples went through the single-stage cascade impactor (SSCI) and processed by high-resolution transmission electron microscopy (HR-TEM) coupled with X-ray microanalysis software (Alderton 2021), using energy-dispersive X-ray spectroscopy (EDS). After, a secondary ion mass spectrometry (ToF–SIMS) was used to analyze the general surface composition of the samples, enabling the analysis of secondary ions (Sjövall et al. 2021). The use of EDS enabled analyses within the scope of analytical chemistry, which increases the precision of studies aimed at identifying the characteristics of the chemical elements present in NPS and ultrafine particles with high resolution (Alencar et al. 2022; Hamdan et al. 2023). According to Quevedo et al. (2020) and Romanovski et al. (2022), direct analysis using HR-TEM consists of the most appropriate method to assess NPs, in addition to preparation by FIB-SEM/EDS.

After detecting the presence of dangerous chemical elements with the analyses carried out in the field, the use of satellite images becomes necessary to understand the displacement of particles suspended in the atmosphere as NPs and ultrafine particles (Neckel et al. 2023). This allows a more complete assessment of the quantity of particulates containing chemical elements capable of moving across large regions (Guleria and Chand 2020; Cappelletti et al. 2022; Neckel et al. 2023).

Method for identifying atmospheric aerosols using Sentinel-3B SYN satellite images

Sentinel-3B level 2 (SYN) satellite images were selected from the ONDA Catalog, made available by ESA, linked to the Copernicus Program (ESA 2023a, 2023b, 2023c). Images from the Sentinel-3B SYN satellite were selected for collection in the following periods: 04–12-2019; 05–08-2019; 23–03-2020; 24–08-2020; 02–13-2021; 25–07-2021; 26–02-2022; 10–28-2022. The Sentinel-3B SYN satellite images followed periods close to field collections of particulate matter by SMPS in this study. The constant presence of cloud shadows made it difficult to select the Sentinel-3B satellite images for the exact SMPS samples. This event is frequent in other studies as well (Zoheir et al. 2019; Neckel et al. 2023).

The Sentinel-3B SYN satellite images used in this study were classified and normalized to a standard average of 0.83 µg/mg, at moderate spatial resolution (260 m), being made available through the researcher login required by the Earth Observation (EO) Sentinel-3B SYN satellite, with operational services from the Global Monitoring for Environment and Security (GMES) carried out by the ESA (ESA 2023a, 2023b, 2023c). The Sentinel-3B SYN satellite images used in 2022 are unpublished, being made available to the researcher's restricted login, attributed exclusively to this study. In each of the Sentinel-3B SYN satellite images used in the periods of 2019–04-12, 2019–08-05, 2020–03-23, 2020–08-24, 2021–02-13, 2021–07-25, 2022–02-26, and 2022–10-28, 634 collection points were selected for the identification of Aerosol Optical Thickness (T550) quantities. Criterion was shortwave infrared (SWIR) with a wavelength of 550 nm, satellite images from Sentinel-3B SYN provided by ESA at a maximum error of 6.62%. When compared to error in the studies by Putra et al. (2022), Zhang et al. (2022), and Wölk et al. (2023), it is noted that the error value exiled a maximum error of 10 to 39.5%. This demonstrates greater reliability of the methodological technique used in this study, when a maximum error of 6.62% is assumed (ESA 2023b, 2023c). ESA (2023a, 2023b, 2023c) emphasizes that the satellite identifies aerosol particles suspended in the atmosphere over a given terrestrial environment, generating a macro-analysis at a spatial resolution of 260 m, which corresponds to greater precision in relation to of the study, as it analyzes the city in its entirety, containing the same properties and sizes of dispersed particulates collected by SMPS via land (Oliveira et al. 2021; Neckel et al. 2023).

The distribution of the 634 sample points by Sentinel-3B SYN satellite images was based on the quantitative distribution of the Triangulated Irregular Network (TIN) (Bartholdi and Goldsman 2004; Zheng et al. 2017). The aim was to encompass the entirety of the internal area of the city of Porto Alegre. According to Racoviteanu et al. (2007) and Zheng et al. (2017), continuous distribution of triangular points with irregular patterns of spacing between the points was optimal. Measurements were spaced from 300 to 500 m apart from the 634 points sampled based on the Sentinel-3B SYN satellite images and collected from the Sentinel Application Platform (SNAP) software v.8.0 by ESA (2023a, 2023b, 2023c). With this it was possible to generate a wavelength database, with a measurement of 550 nm of T550, stored in electronic spreadsheets. Using SNAP software (ESA 2023a, 2023b, 2023c), the images selected from the ONDA catalog were cropped in relation to the area of influence of this study (the city of Porto Alegre) and re-projected. Subsequently, utilizing SNAP software, geospatial data were collected using the point management tool (ESA 2023a, 2023b, 2023c). Thus, it was possible to generate a database

referring to the SYN Aerosol Optical Thickness (T550) and store it in electronic spreadsheets.

This spreadsheet was analyzed using JASP software (Jeffrey's Amazing Statistics Program—version 0.14.1.0), which enabled K-means cluster analysis. This analysis obtains vector data with representative clusters based on the centroid, which consists of the geometric center of the most representative clusters generated from the average originated by the Silhouette index, determined by the average grouping of the clusters (Batool and Hennig 2021; Maroni et al. 2021; Qv et al. 2022). These K-means groupings, based on Eq. (1), according to Dal Moro et al. (2021), contain the representation of distance (d) considering each of the points, based on the point of a cluster (p_i), where the total elements ($x\{x_1, x_k\}$) are identified, in addition to considering the number of elements (n), provided from the data collected in the 634 points sampled using the Sentinel-3B SYN images. Subsequently, Eq. (2) was applied, consisting of the sum squared error (SSE), considering the squared error based on the total elements (N_i) and elements (X_{ij}), in addition to the centroid point (C_i) (Leong et al. 2020; Brunner et al. 2022). The SSE consists of a measure of precision of numerical data of similar magnitude, where the errors, after being squared, were added constituting the high precision of the data prediction model (Leong et al. 2020; Brunner et al. 2022) sampled from Sentinel-3B SYN satellite images (Neckel et al. 2023). The results of Eq. (2) were applied in Eq. (3), where the average of all data in the group ($S(i)$) and the minimum distance ($b(i)$) is taken into account along with other sampled data that do not belong to the group. Group (i), taking into account the average distance of data ($a(i)$) aimed at optimizing vector data, is responsible for the formation of clusters (Dal Moro et al. 2021; Neckel et al. 2023).

$$d(p,x) = \frac{1}{n}\sum_{i=1}^{n} \mathrm{d}(p_i,x)^2 \tag{1}$$

$$\mathrm{SSE2} = \frac{N_i \Sigma_j \| x_{ij} - c_i \|^2}{N_i - 1} < \mathrm{SSE1} = \frac{N_1 \Sigma_j \| x_{1j} - c_1 \|^2}{N_1 - 1} \tag{2}$$

$$S(i) = \frac{b(i) - a(i)}{\max(a(i), b(i))} \tag{3}$$

After applying the Silhouette index containing the average groupings of the clusters obtained in this study, the properties of the numerical means obtained from the categorized groupings were considered. Values greater than 1 demonstrate high reliability attributed to the results of the clustering groups. Values lower than − 1 support a non-correlation of coherence between the results acquired from the clusters (Naghizadeh and Metaxas 2020; Kariyam et al. 2023). Dal Moro et al. (2021) emphasize the need to apply clusters in applied research. This allows for a more adequate graphical understanding of the results obtained by the reader, justifying the importance of the methodological application of clusters in this study. Clusters extracted from 550-nm data (T550) of the Sentinel-3B SYN images.

Results and discussion

Samples by SMPS

The results of this study identified by EDS, as recommended by Alderton (2021), made it possible to analyze 3837 NPs and ultrafine particles from the 32 points sampled in the urban area of the state capital city of Porto Alegre, in addition to the detection of the most abundant minerals: quartz, clays, hematite, and gypsum (e.g., Fig. 3). Some authors (Lu et al. 2016; Kumar et al. 2022) stated that the presence of quartz, hematite, and gypsum in particulate matter correspond to neoformed structures and nanominerals originating from the combustion of fossil fuels associated with chemical elements that suffered oxidation. These are transformed into carbonates, aluminosilicates, phosphates, and sulfides, thus composing complex atmospheric geochemical reactions including massive amounts of amorphous materials.

Table 1 demonstrates the great variety and complexity of the amorphous and mineralogical phases present in the samples obtained in this study. These obtained data can easily be classified into five major groups: (1) soot aggregates; (2) organometallic; (3) organic amorphous; (4) inorganic amorphous; (5) minerals, when related to other studies (Oliveira et al. 2021; Silva et al. 2022; Neckel et al. 2023).

Through the analysis carried out using Tof–SIMS, it was demonstrated that aluminum and iron had a similar distribution pattern, except for some particles composed mainly of aluminum and silicon (clay particles). By evaluating the results of Tof–SIMS with FE-SEM and HR-TEM, we can ratify the great diversity of chemical and mineral elements present in the area under study (Table 1). In Fig. 4, it becomes possible to observe that in the red color there are no color changes, which is observed only in some particles, but in the rest of the image (Fig. 4) the red color changed to orange, indicating that there is a mixture of aluminum, silicon, and iron. Consequently, in existing chemical elements with particles close to the intense orange color, the indication is that these particles are very abundant (Perrotti et al. 2019; Zhou et al. 2023). The overview by ToF–SIMS later helped in the analysis of electron microscopy. Therefore, the methodology used is considered by the authors to be efficient and robust so that they can be used in several other areas for air quality studies. After all, several toxic elements such as arsenic (As), cadmium (Cd), chromium (Cr), and lead (Pb) were associated in amorphous phases of (aluminum) Al and iron (Fe), originating from the greater geochemical

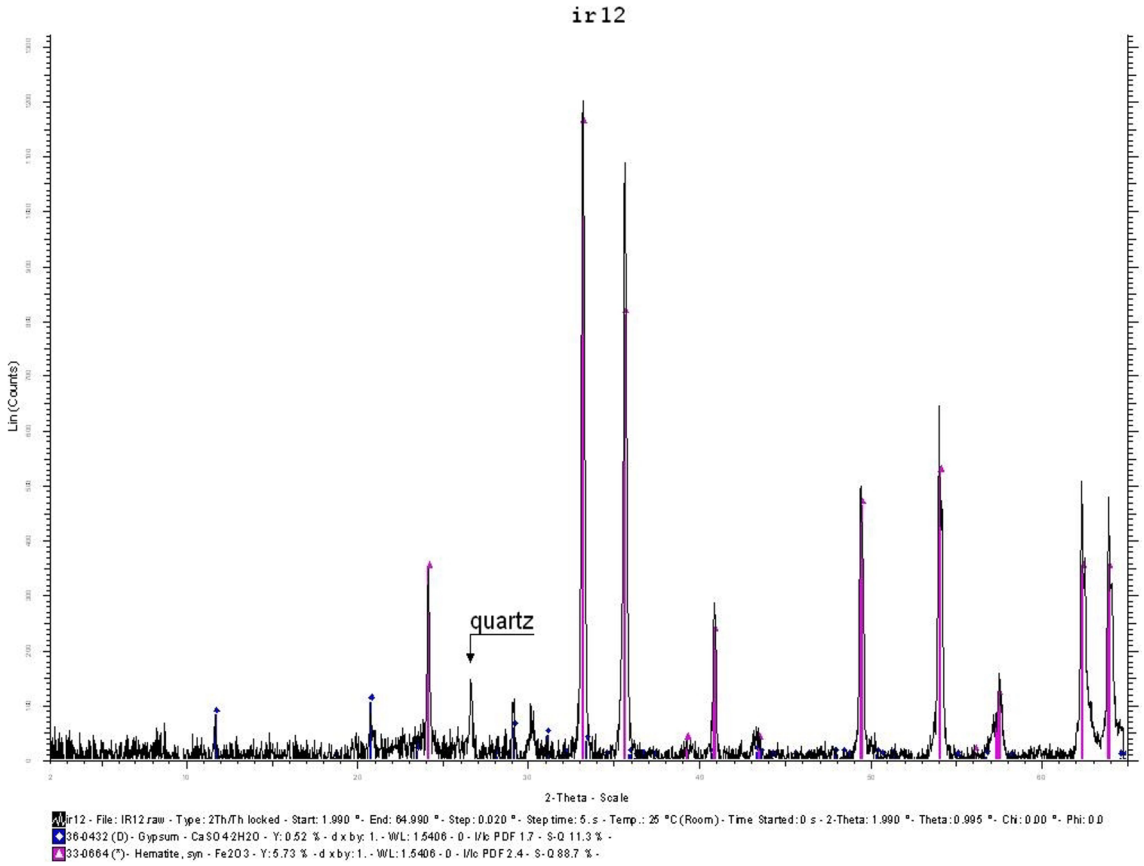

Fig. 3 Homogenized proportion of the presence of the main most abundant minerals (quartz, hematite, and gypsum)

relationships between the toxic elements detected in this study. Al and Fe, together with NPs and ultrafine particles, when associated, become more reactive when integrated into the environment, in addition to containing greater proportions of hazardous elements. Therefore, they have the potential to cause greater harm to human health than air pollution (Oliveira et al. 2021; Silva et al. 2022; Zhu et al. 2023). These interactions were also detected in the presence of Fe minerals (e.g., hematite, magnetite, and goethite) and Al, in addition to having multiple associations with organic phases detected by HR-TEM, FE-SEM, and especially by ToF–SIMS (Fig. 5).

It should be noted that the samples obtained showed very complex mineralogical compositions. This is likely due to the pollutants released by intense industrial activities in the area under study. Furthermore, asphalt wear due to heavy traffic releases NPs and ultrafine particles into the atmosphere. Due to their low density, these particles remain suspended for long periods of time (Tang et al. 2020; Ketzel et al. 2021; Marcella et al. 2022). Similar results were reported by several studies that utilized SMPSs (Herrera and Videla 2009; Morillas et al. 2019). It can be proven using FE-SEM and HR-TEM that particles larger than 10 µm were more abundant when it comes to minerals, such as quartz, clays, and carbonates. NPs, on the other hand, were mainly composed of amorphous compounds and minerals such as oxides and hydroxides.

The SMPS samples contained a higher proportion of organic particles and sulfates compared to the road dust samples. This is understandable given that samplers were located at a height of 1.5 m above the sidewalk. This height was chosen as it is roughly the height at which air would be taken into the body by the average pedestrian in the study area. Less dense road dust particles were found in these samples (Xu et al. 2017; Oliveira et al. 2021; Zou and Yang 2022). With this, it can be seen that the health of the population that transits through the busiest central area of the city of Porto Alegre, as well as building materials, are more exposed to sulfates and organic compounds derived particularly from motorized vehicle traffic, but also from the presence of railways and industry on site.

Table 2 consists of the representation of the main hazardous elements detected in the NPs and ultrafine particles of this study, according to size. It is observed that while the particles larger than 10 µm mostly contain chemical elements such as Si, Al, K, Na, Fe, Mg, P, and Ti (derived

Table 1 Amorphous phases and minerals detected by electron microscopies

	SMPS	SSCI	Road dust
Fullerenes (C_{60}, C_{70}, C_{80})	▲	▲	▲
Amorphous inorganic phases	▲	▲	▲
Amorphous organic nanophases	▲	▲	▲
Silicates			
Quartz, SiO_2	▲	▲	▲
Chlorite, $Na_{0.5}Al_6(Si,Al)_8O_{20}(OH)_{10}{\cdot}H_2O$	▼	▲	▲
Illite, $K_{1.5}Al_4(Si_{6.5}Al_{1.5})O_{20}(OH)_4$	▲	▲	▲
Kaolilite, $Al_2Si_2O_5(OH)_4$	▲	▲	▲
Microcline, $KAlSi_3O_8$	▼	▲	▲
Mullite, $Al_6Si_2O_{13}$	▼	▲	▲
Muscovite, $KAl_2(AlSi_3)O_{10}(OH)_2$	▼	▲	▲
Zircon, $ZrSiO_4$	▼	▼	▲
Carbonates			
Calcite, $CaCO_3$	▼	▲	▲
Dolomite, $CaMg(CO_3)_2$	▼	▲	▲
Siderite, $FeCO_3$	▼	▲	▲
Sulfates			
Ammoniojarosite, $[(NH_4)Fe_3(SO_4)_2(OH)_6]$	▼	▼	▼
Anhydrite, $CaSO_4$	▲	▲	▲
Alunogen, $Al_2(SO_4)_3{\cdot}17H_2O$	▼	▼	▲
Alunite, $(K,Na)Al_3(SO_4)_2(OH)_6$	▼	▼	▲
Barite, $BaSO_4$	▲	▲	▲
Epsomite, $MgSO_4{\cdot}7H_2O$	▼	▼	▲
Hexahydrite, $MgSO_4{\cdot}6H_2O$	▼	▼	▼
Gypsum, $Ca[SO_4]{\cdot}2H_2O$	▲	▲	▲
Jarosite, $KFe^{3+}{}_3(SO_4)_2(OH)_6$	▼	▼	▼
Natrojarosite, $NaFe_3(SO_4)_2(OH)_6$	▼	▼	▼
Pickeringite, $MgAl_2(SO_4)_4{\cdot}22H_2O$	▼	▼	▼
Oxides and hydroxides			
Anatase, TiO_2	▲	▲	▲
Brookite, TiO_2	▲	▲	▲
Chromite, $(Fe,Mg)Cr_2O_4$	▼	▼	▲
Hematite, Fe_2O_3	▲	▲	▲
Goethite, $Fe(OH)_3$	▲	▲	▲
Gibbsite, $Al(OH)_3$	▲	▲	▲
Magnetite, Fe_3O_4	▼	▲	▲
Rutile, TiO_2	▲	▲	▲

especially from soil and asphalt wear), the particles between 1 and 100 nm contain less of these elements and more elements potentially toxic to the environment and to human health. This clearly indicates that they are mainly derived from anthropogenic activities. Previous studies (Oliveira et al. 2021; Silva et al. 2022) have shown that NPs and ultrafine particles are mostly composed of organic compounds, sulfates, and amorphous phases. It should also be noted that such NPs are extremely easy for the human body to adsorb (Oliveira et al. 2021; Silva et al. 2022).

Table 3 becomes of great importance when demonstrating the main sources of emissions of identified contaminants in the area under study. In addition, it presents possible hot spots to the scientific and civil communities that need a greater degree of management by governments and public managers. According to Bodah et al. (2022) and Li (2023), a possible solution to this issue is the creation of public policies capable of subsidizing future urban restoration projects aimed at environmental recovery. The combined use of urban vegetation and trees together with inspections capable of identifying irregular gas emissions by automotive vehicles and polluting industries was shown to have a measurable impact on localized environmental quality.

In all samples obtained in this study, spherical particles of multiple sizes were detected (Fig. 6). The most likely sources of these pollutants were emissions from coal-fired power plants and wear and tear from urban construction materials (Silva et al. 2022). Knowing that coal fly ash is a widely used ingredient in the production of cement in the area under study, and that there is an abundance of cement production facilities in the city, it can be concluded that these are the main sources of ultrafine particles. Fines containing high proportions of the hazardous elements arsenic (As), silver (Ag), barium (Ba), bromine (Br), cadmium (Cd), chlorine (Cl), cobalt (Co), copper (Cu), chromium (Cr), fluorine (F), gallium (Ga), mercury (Hg), lithium (Li), manganese (Mn), molybdenum (Mo), niobium (Nb), nickel (Ni), lead (Pb), palladium (Pd), sulfur (S), antimony (Sb), selenium (Se), scandium (Sc), tin (Sn), vanadium (V), titanium (Ti), and zinc (Zn) were analyzed in this study.

Tables 1, 2, and 3 help to demonstrate the complexity of the particulate matter in the area under study. Among the most important phases found by FE-SEM and HR-TEM, the amorphous phases stood out due to their significant capacity to adsorb toxic elements such as Cd and Cr (Fig. 7). For Silva et al. (2022) and Tian et al. (2023), the complexity of amorphous phases has fascinated geochemical scientists in recent decades, especially due to their great diversity and high reactivity with organic and inorganic contaminants. Although some minerals such as oxides and hydroxides of Fe and Al also showed high adsorption of toxic elements, the amorphous phases contained a greater amount of hazardous compounds associated in the present study.

Both samples collected by SMPSs and those obtained by SSCI had similar morphologies and chemical compositions for particles smaller than 100 nm. In general, Table 2 represents most of the compounds detected in particles smaller than 100 nm. Figure 8 illustrates their composition, with a total of 1824 nanoparticles collected via SMPS and 2013 nanoparticles detected with SSCI identified and analyzed. Through Fig. 8, it is easily observed that particles smaller than 100 nm sampled by SMPS and SSCI mostly contained carbon. This, according to several studies (Herrera and

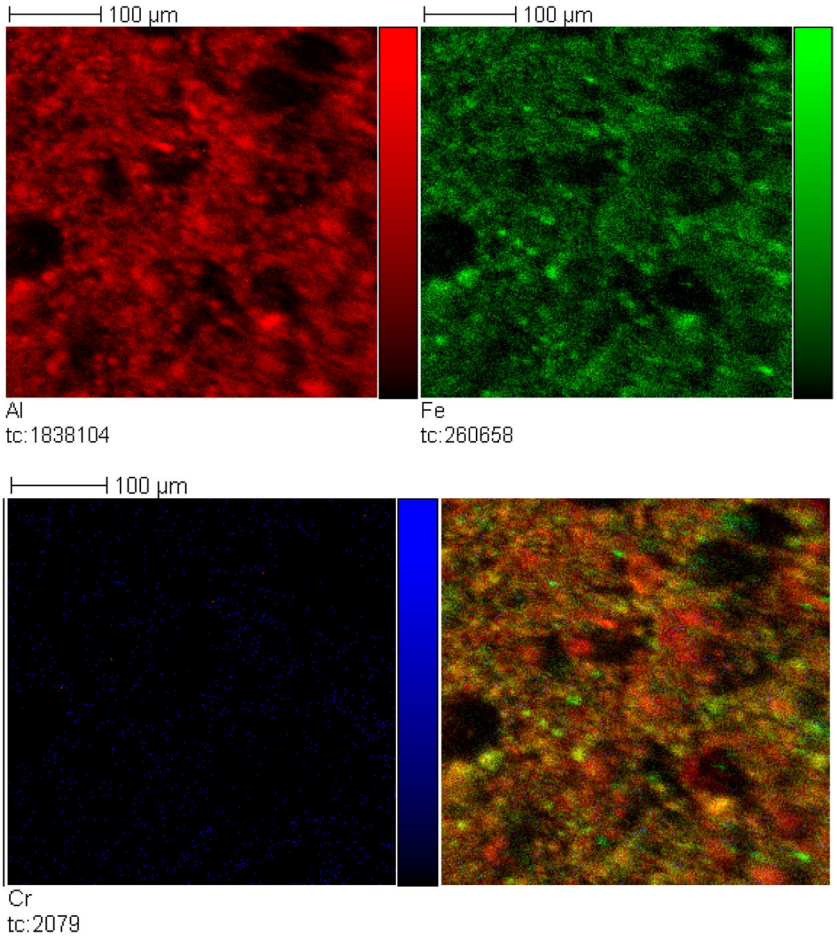

Fig. 4 Result of homogenized samples of particles suspended in the atmosphere collected from SMPS, being analyzed via ToF–SIMS

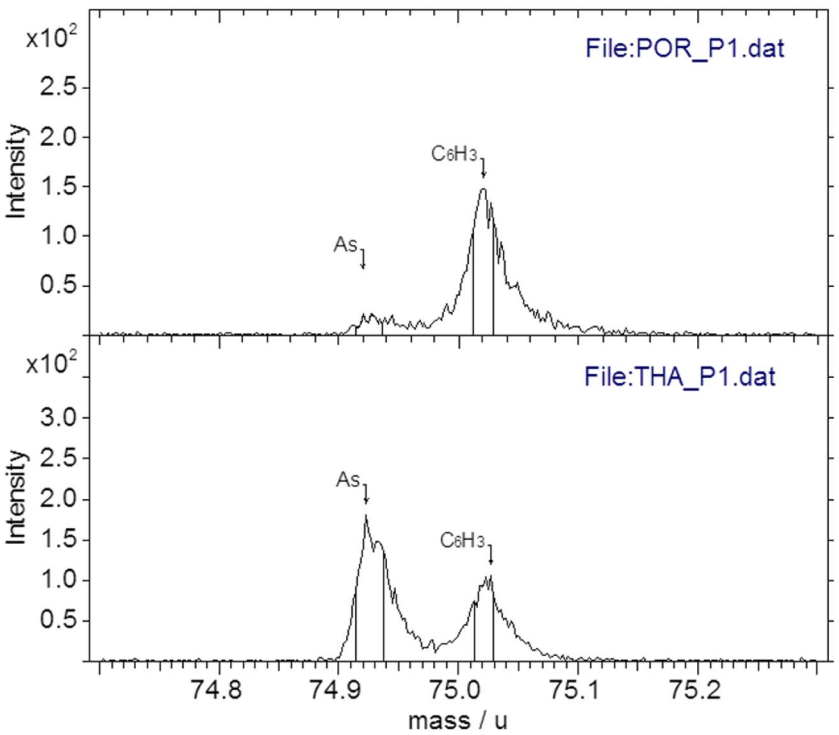

Fig. 5 Detection of multiple associations with organic phases via HR-TEM, FE-SEM, and ToF–SIMS

Table 2 Principal hazardous chemical elements detected by EDS coupled with HR-TEM and FE-SEM

EDS coupled	> 10 µm	5–10 µm	1–5 µm	0.1–1 µm	1–100 nm
SSCI, SMPS, and road dust	Cl, Cr, Mn, Ni, Pb, Pd, S, Ti, V, Zn	Cl, Cu, Cr, Mn, Ni, Pb, Pd, S, Ti, V, Zn	Cl, Co, Cu, Cr, Mn, Ni, S, Pb, Pd, Ti, V, Zn	Ba, Cl, Co, Cu, Cr, Mn, Ni, S, Sb, Sn, Pb, Pd, Ti, V, Zn	As, Ag, Ba, Br, Cd, Cl, Co, Cu, Cr, F, Ga, Hg, Li, Mn, Mo, Nb, Ni, Pb, Pd, S, Sb, Sc, Se, Sn, Ti, V, Zn

Videla 2009; Morillas et al. 2019; Silva et al. 2022; Neckel et al. 2023), indicates that these are organic or organometallic particles that may or may not contain dangerous elements such as Cd, V, Se, Pb, Mo, Sb, and Sn, among many others detected by EDS coupled to HR-HE HAS. Figure 8 also demonstrates that sulfur compounds (mostly sulfates) were detected in very abundant proportions, as well as nanoparticles of Al, Si, Mg, K, and Na (such elements present both as minerals and as amorphous phases). In this ratio of abundance in mineral and amorphous structures (Fig. 8), some dangerous elements detected in NPs and ultrafine particles are added (Table 2). This makes the applicability of remote sensing with the use of satellite images a priority to assess whether these atmospheric contaminants in the form of NPs and ultrafine particles are stationary or are expanding to large regions in different seasons of the year, as shown by the collection periods by SMPS (Bodah et al. 2022; Balch and Mitchell 2023).

Dynamics of atmospheric aerosols by Sentinel-3B SYN satellite images at macroscale in the city of Porto Alegre

The macroscale distribution of the TIN covered the urban area of the city of Porto Alegre. The T550 data collection points, distributed from the Sentinel-3B SYN satellite images, covered an even larger region when compared to the area of the Centro Histórico (Historical Center) neighborhood where particulate samples were collected using SMPSs. According to Bodah et al. (2022), the collection of satellite data on macroscales makes it possible to understand the dynamics of both the existence of and movements of atmospheric aerosols.

The results of this study demonstrate that the highest T550 averages occurred during the years 2019 (0.392) and 2020 (0.248) (Table 4). The maximum T550 value identified occurred in 2019 (0.620) and the lowest minimum value occurred in 2020 (0.070) (Table 4). Thus, it becomes visible to identify the occurrence of the quantitative reduction of T550 in the year 2022, when compared to the years 2019, 2020, and 2021. This reduction of T550 can be attributed to the statements presented by the Brazilian Agency of Geography and Statistics (IBGE 2023), which highlights that 3.4 million companies operate in the entirety of Brazil. Of this total, 845,717 companies are located in the State of Rio Grande do Sul (of which Porto Alegre is the capital). Greater than 42% (42.9%) reported that they suffered negative impacts in activity throughout the duration of the COVID-19 global pandemic. This included drastic reductions in the release of aerosols into the atmosphere during this time. Aerosols are particulates that potentially contain elements that are dangerous to the environment and to human health. According to data from the Department

Table 3 Principal types of ultrafine particles (< 0.1 μm) in sampled particulate matter based on electron microscopies

Types of ultrafine particles	Morphologies	Principal sources
Minerals	Core–shell structure; Irregular	– Fuel and biomass burning – Soil – Road dust – Constructions materials – Coal power plants
Organometallic	Irregular morphologies Spherical/near-spherical Chain-like Cluster-like Compact-like	– Emission of boats and vehicles burning fossil fuel – Coal power plants
Organic amorphous compounds	Irregular morphologies Spherical/near-spherical Chain-like Cluster-like Compact-like	– Secondary conversion of volatile organic compounds – Mixture of secondary particles and primary ultrafine particles are formed by heterogeneous geochemical interactions – Industrial emissions – Coal power plants
Soot aggregates	Irregular Spherical/near-spherical Chain-like Cluster-like Compact-like	– Emission of boats and vehicles burning fossil fuel – Coal power plants – Coal power plants
Inorganic amorphous compounds	Irregular	– Soil – Road dust – Construction materials – Coal power plants

of Economic Development of Brazil, the effects of the COVID-19 pandemic led to the permanent dissolution of 70,842 companies in the state of Rio Grande do Sul by 2021, some of which had polluting characteristics (SDE 2023). This decrease in atmospheric aerosols due to the suspension of some polluting industrial activities contributes to the mitigation of harmful impacts on the environment and human health (Mandal and Patel 2021; Liang et al. 2023).

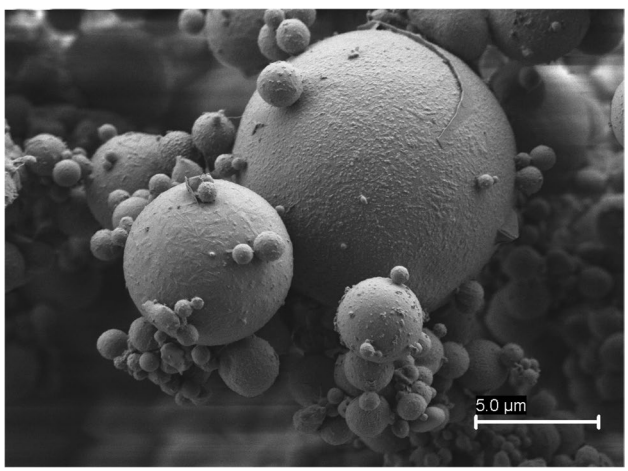

Fig. 6 Detection of spherical particles of multiple sizes of particles suspended in the atmosphere analyzed

T550 data collected by the Sentinel-3B SYN satellite images was submitted for K-means analysis utilizing a statistical adjustment model (Naghizadeh and Metaxas 2020; Kariyam et al. 2023). In this dataset, $K = 12$ were the dataset groupings with the number of 634 points collected from the Sentinel-3B SYN satellite images in 2019, 2020, 2021, and 2022. According to Dal Moro et al. (2021) and Neckel et al. (2023), the R^2 consists of the ratio present in the sums and total squares. The closer the value is to 1.0, the greater the "goodness of fit," a statistical representation of how well the data line up with the expected distribution. High values demonstrate greater reliability of the data modeled in the research. In this study, the observed value of R^2 was 0.813, demonstrating that the model presents an adequate answer to the questions posed in this research by presenting a greater statistical reliability. The Akaike Information Criterion (AIC) presented a value of 1141.390, while the Bayesian Information Criterion (BIC) generated a total of 1568.780 when measuring the "goodness of fit" of this statistical model (Mehrjou et al. 2016; Dal Moro et al. 2021; Li et al. 2022), which again demonstrates greater reliability of the data collected in this study. In this context, the silhouette index ranged from zero (0) to one (1); and the $K = 12$ clusters yielded a result of 0.320 in relation to the clustering tendency of the clusters, according to the variables established in this study. The silhouette index of 0.320 identified in this study is similar to the research by Neckel et al. (2023),

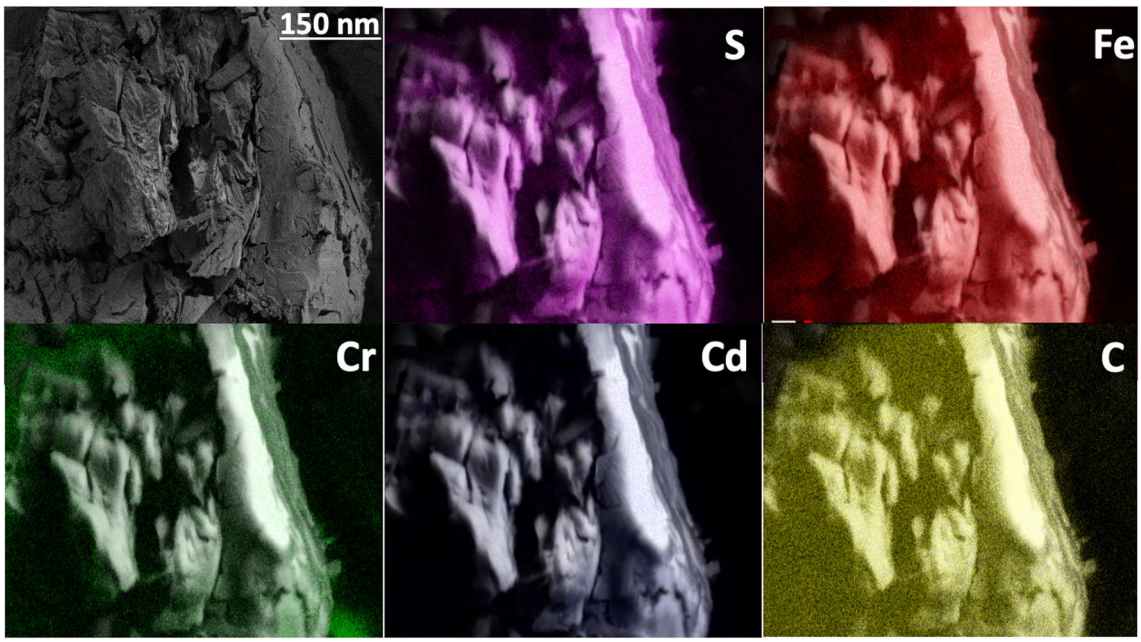

Fig. 7 Higher major importance detected by FE-SEM and HR-TEM in amorphous phases

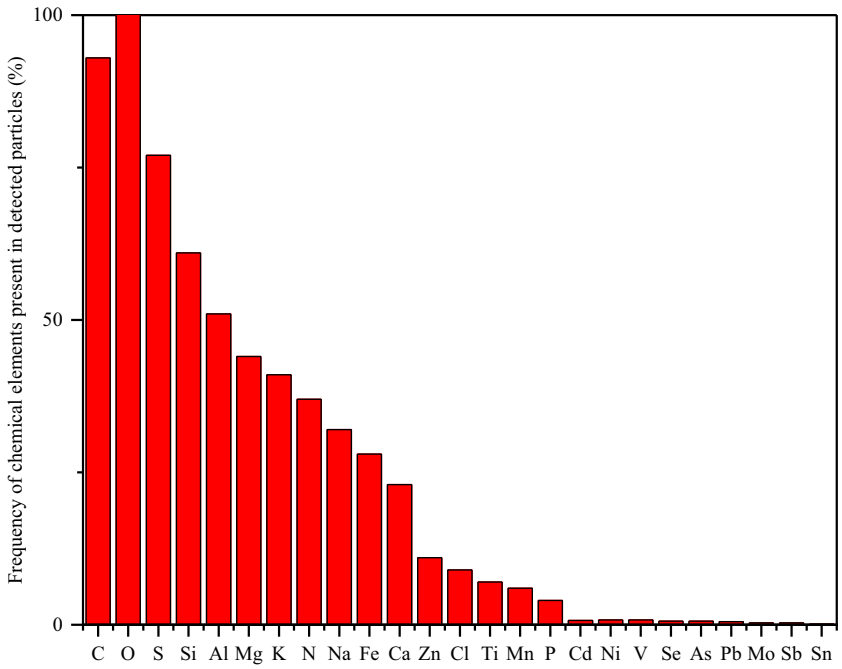

Fig. 8 Samples collected by SMPS, obtained by SSCI, with similar morphologies and chemical compositions in particles smaller than 100 nm

which correspond to $K=5$ over a silhouette index of 0.360. This demonstrates the safety of the statistical application in this study, in relation to the other study (Neckel et al. 2023) when working with geospatial analyses in similar statistics, through the data collected in the Sentinel-3B SYN satellite images (Table 5).

Through Table 5, it becomes possible to represent the sizes of the clusters, in addition to the individual variability of each one of the clusters in relation to the sum of squares, with the proportion of internal heterogeneity of the cluster and the Silhouette index. It must be remembered that the heterogeneity of a cluster consists of the total value corresponding to 1, when divided proportionally (Dal Moro et al. 2021; Zequan et al. 2022). According to Mehrjou et al. (2016) and Zequan et al. (2022), grouping by clusters enables researchers worldwide to carry out analyses with a high

Table 4 Descriptive statistics of average T550 data collected from Sentinel-3B SYN satellite images

Statistical items	Winter 2019	Summer 2019	Winter 2020	Summer 2020	Winter 2021	Summer 2021	Winter 2022	Summer 2022
Valid	634	634	634	634	634	634	634	634
Absent	0	0	0	0	0	0	0	0
Average	0.110	0.392	0.096	0.251	0.248	0.192	0.264	0.228
Standard deviation	0.012	0.087	0.024	0.027	0.044	0.047	0.123	0.033
Minimum	0.085	0.094	0.070	0.193	0.094	0.109	0.100	0.109
Maximum	0.149	0.620	0.323	0.333	0.425	0.338	0.574	0.329

Table 5 Cluster statistical information generated from the data collected in the Sentinel-3B SYN satellite images

Items	Clusters											
	1	2	3	4	5	6	7	8	9	10	11	12
Cluster size	13	123	55	60	92	68	5	38	42	37	43	38
Proportion of heterogeneity within the cluster	0.052	0.109	0.051	0.052	0.099	0.177	0.023	0.130	0.028	0.104	0.061	0.115
Sum of squares	49.398	103.264	48.263	49.035	94.293	168.265	21.583	123.171	26.384	98.456	58.252	109.022
Silhouette index	0.344	0.307	0.418	0.286	0.343	0.276	0.641	0.368	0.427	0.191	0.294	0.240

degree of sample reliability in different surveys. Cluster 2 (Table 5) presented, in relation to 123 collection points demonstrated in this study, a heterogeneity of 0.109. Cluster 6 showed greater homogeneity, with 68 points and a proportion of 0.177, followed by cluster 7, which had the lowest number, corresponding to 5 collection points, with the least heterogeneity with a total of 0.023.

Another capable parameter used to evaluate the cluster consists of the sum of squares (Dal Moro et al. 2021; Zequan et al. 2022). The smaller the sum of squares, the smaller the variability of results from sampling becomes (Novo et al. 2022; Huaji et al. 2023). In this relationship, cluster 6 had the highest sum of squares, totaling 168,265. Cluster 7 had the lowest sum of squares, totaling 21,583, demonstrating high homogeneity and reliability in relation to the results analyzed in this study. The Silhouette index demonstrated homogeneity and cohesion, where the best results were from cluster 7 with an index of 0.641. Cluster 10 presented the lowest index of 0.191 (Table 5). This study demonstrates the existence of significant homogeneity between the values of each cluster. According to Dal Moro et al. (2021) and Novo et al. (2022), the use of cluster analysis, based on an understanding of the significance of research, raises the degree of reliability of the modeled results to the level of excellence.

Regarding Gaussian kernel density (Fig. 9), smoothed from canopy height distributions (>0 m) based on a stratified random sample from each cluster (Dal Moro et al. 2021; Neckel et al. 2023), each cluster has a specific pigmentation. The caption is able to describe in detail the attributions of these representative colors assigned to the clusters. Through this, it becomes possible to visualize the densities of the clusters in each average density variable along with their overlaps (Fig. 9). The variables that most contributed to the grouping of the clusters is shown in Table 6. At their midpoint, the authors observed the scope and its relationship with each statistical variable analyzed. Note that cluster 8 had the highest values, especially during the winter of 2019 (2.684) and 2021 (2.549). The lowest values showed the greatest variation in cluster 3, with a high influence in the winter of 2019 (−1.693) and in the summer of 2022, where it totaled 1.637.

This study demonstrates that as of 2019, the concentration of aerosols in the city of Porto Alegre has been reduced (Fig. 10). Winter 2019 and winter 2021 showed the highest concentrations of aerosols in and around the city of Porto Alegre (Fig. 10A and E), but in the winter of 2020, the lowest concentration of aerosols occurred (Fig. 10C). In 2021, it was possible to verify the decrease in T550 levels, both in winter and in summer (Fig. 10G and H). This cluster analysis demonstrates a separation in aerosol concentrations according to the region of the city of Porto Alegre (Fig. 11), which can be observed in central Porto Alegre. Cluster 8 presented high elevations in the levels of T550 and cluster 3 presented the lowest levels of T550. Cluster 3 is located in the most wooded central area of the city. According to Teixeira et al. (2022) and Vithanage et al. (2022), it is necessary to maintain, implement, and preserve urban vegetation in order to reduce hazardous atmospheric elements. The hazardous elements identified in this study were Si, Al, K, Mg, P, and Ti. Each was collected in the field using SMPSs

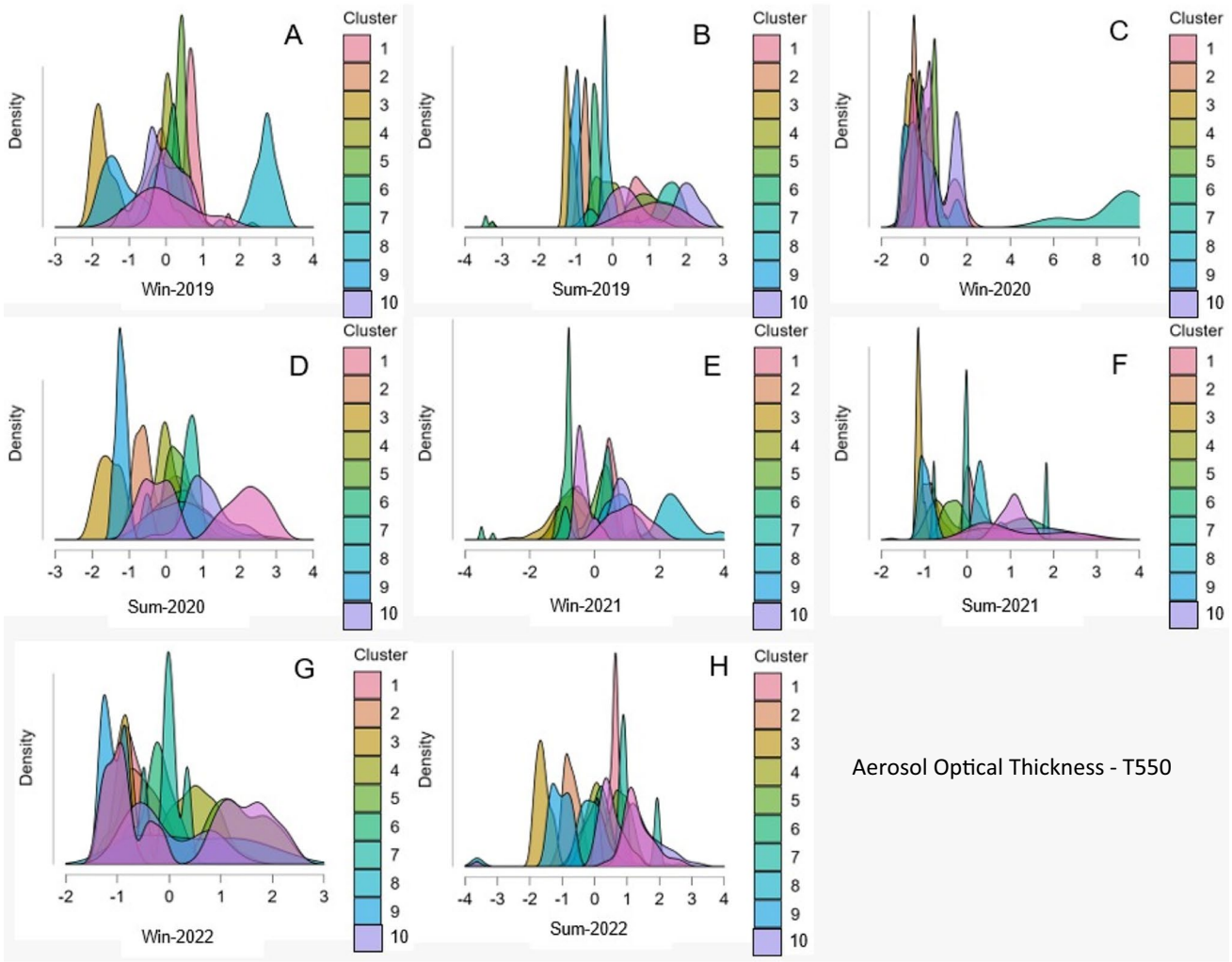

Fig. 9 Average density of clusters analyzed by Gaussian kernel density from data collected in Sentinel-3B SYN satellite images

Table 6 Average clusters generated from data collected in Sentinel-3B SYN satellite images

Clusters	Winter 2019	Summer 2019	Winter 2020	Summer 2020	Winter 2021	Summer 2021	Winter 2022	Summer 2022
1	0.700	0.834	0.488	0.509	0.556	0.155	−0.686	0.640
2	−0.219	−0.759	−0.411	−0.589	−0.531	−0.813	−0.561	−0.738
3	−1.693	−1.224	−0.581	−1.531	−0.887	−1.094	−0.927	−1.637
4	0.073	−0.191	−0.076	−0.007	−0.700	−0.514	0.510	−0.018
5	0.422	1.055	0.328	0.354	0.221	−0.201	1.415	0.765
6	0.154	−0.552	−0.228	0.388	−0.896	1.389	−0.278	0.215
7	0.080	1.137	8.810	0.440	0.092	0.191	−0.032	0.927
8	2.684	−0.135	0.285	0.474	2.549	0.388	0.446	−0.257
9	−1.250	−1.006	−0.619	−1.211	0.762	−0.969	−1.074	−1.052
10	−0.378	1.845	1.204	1.085	0.666	1.269	−0.081	1.529
11	0.201	0.377	0.081	−0.273	−0.355	1.060	1.519	0.404
12	−0.034	1.114	−0.544	2.203	1.046	1.115	−0.876	1.345

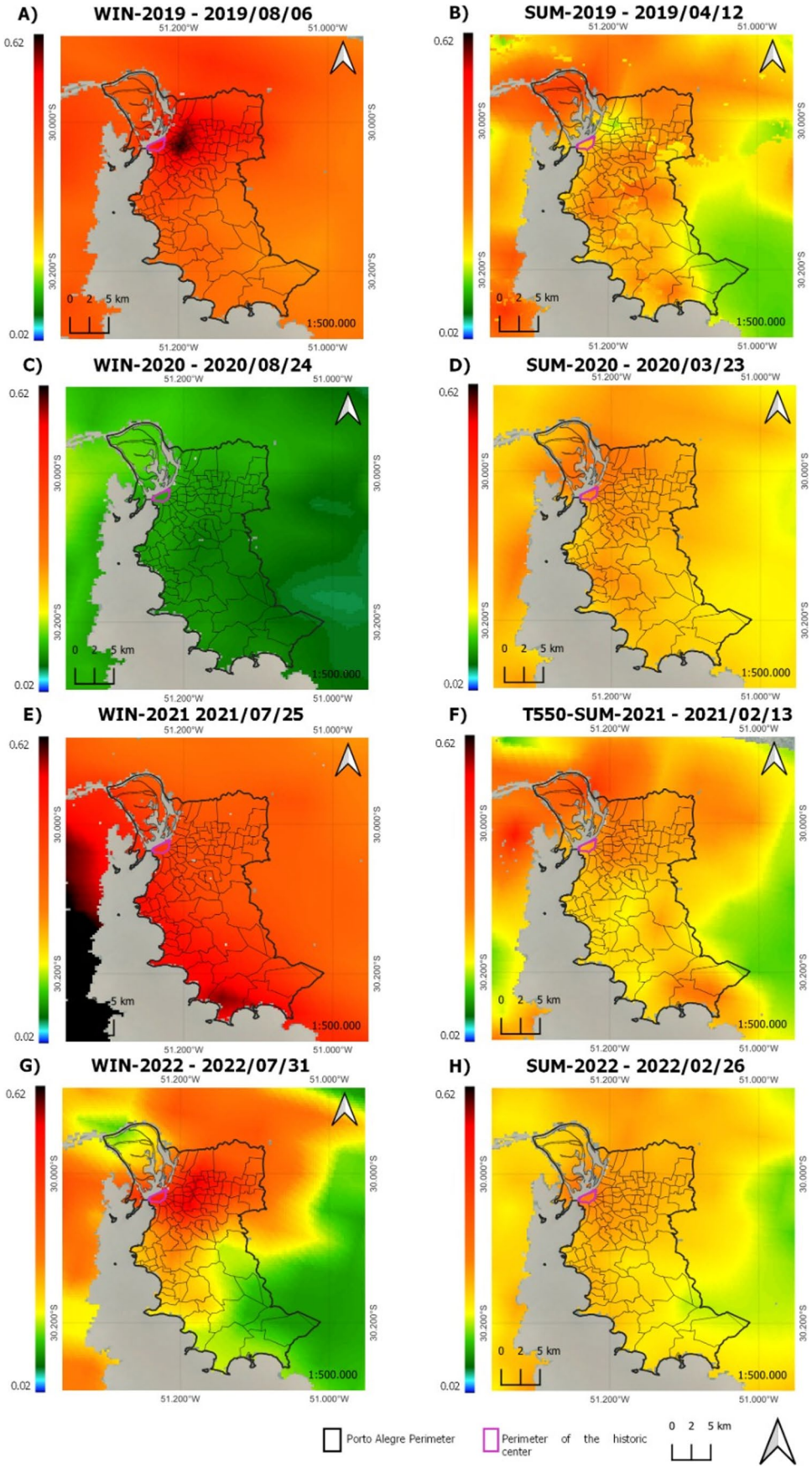

Fig. 10 Quantitative of T550 identified in the city of Porto Alegre (RS) from data collected in satellite images Sentinel-3B SYN

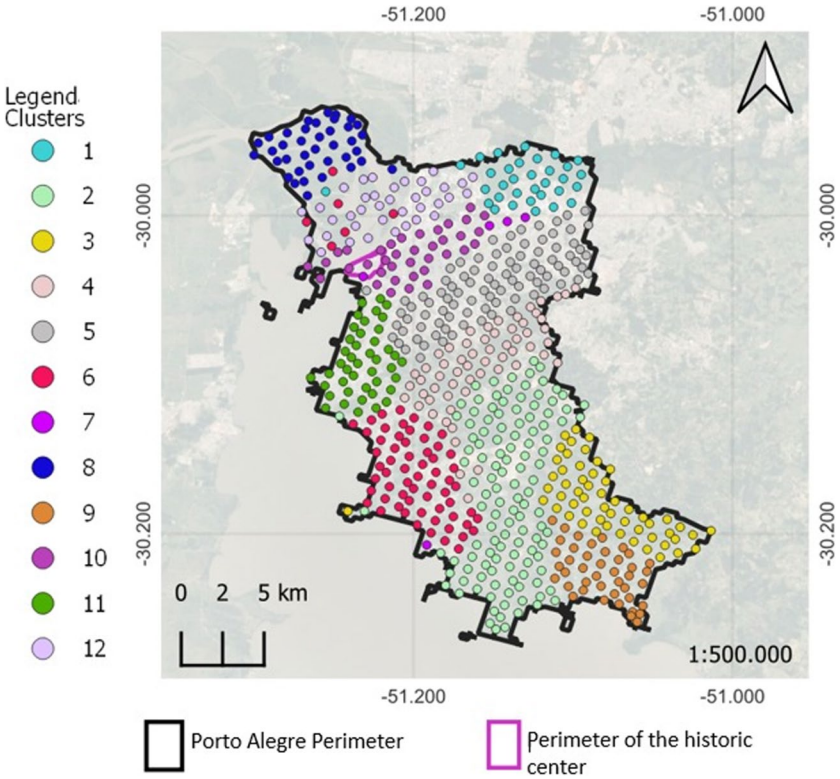

Fig. 11 Grouping of clusters generated from the collection points in Sentinel-3B SYN satellite images in the urban perimeter of the city of Porto Alegre, Rio Grande do Sul, Brazil

in the form of NPs and ultrafine particles suspended in the atmosphere. This can serve as a warning to governments and public managers for the creation of public policies that will contribute to the development of future urban projects aimed at preserving the environment and the quality of life of the population throughout the urban perimeter, as suggested by other studies (Bodah et al. 2022; Neckel et al. 2023). The expansion dynamics of these aerosols (T550), which can contain hazardous chemical elements, are capable of moving to large regions beyond the city of Porto Alegre, as identified by the Sentinel-3B SYN satellite images examined in this study.

Conclusion

Suspended particles examined in this study showed toxic elements present in NPs and ultrafine particles in Porto Alegre's Centro Histórico neighborhood, the city's busiest. This speaks of the need for stricter inspections aimed at identifying sources of pollution in addition to subsidizing new public policies and future projects to revitalize the built environment.

Regarding the collections carried out on a macroscale by images from the Sentinel-3B SYN satellite, the sum of the squares in cluster 6 is a total of 168,265 and in cluster 7 (the same place where particles suspended in the atmosphere by SMPS were collected in terrestrial form) a total of 21,583, demonstrating high homogeneity and reliability in the results of this study. In this context, the importance of using images from the Sentinel-3B SYN satellite to obtain T550 levels is highlighted, as it reveals that atmospheric pollution can move through air currents in the atmosphere contaminating large regions. The decrease of T550 in the study area of the city of Porto Alegre stands out due to the decrease in industrial activity and subsequent pollution during the COVID-19 pandemic. Future avenues of study suggested by the authors include expanding this methodology on a global scale to conduct analyses of suspended particles in the atmosphere and identifying NPs and ultrafine particles by FIB-SEM and HR-TEM. Used in conjunction with Sentinel-3B SYN satellite imagery, a more complete quantitative analysis of the proportions of identified atmospheric aerosols can be achieved.

Acknowledgements The authors thank the European Space Agency (ESA) and the U.S. National Aeronautics and Space Administration (NASA) for providing the unpublished and treated images from the Sentinel-3B SYN satellite, and the NOAA Air Resources Laboratory (ARL) for the provision of the HYSPLIT transport and dispersion model and/or READY website (http://www.ready.noaa.gov) used in this publication. The authors also thank the Center for Studies and Research on Urban Mobility (NEPMOUR+S/ATITUS), Brazil; Fundação Meridional, Brazil; Atlantic International Research Centre (AIR Centre) (https://www.aircentre.org/Scholarship/), Portugal; and the National Council for Scientific and Technological Development (CNPq), Brazil.

Author contribution MGB, LSM, and GTC: conceptualization, funding acquisition. ETB, PCT, LSM, and MLSO: final manuscript writing. AN, BWB, LPL, and LFOS: review and editing.

Funding National Council for Scientific and Technological Development (CNPq).

Declarations

Conflict of interest The authors declare no competing interests.

References

Aarzoo N, Nidhi N, Samim M (2022) Palladium nanoparticles as emerging pollutants from motor vehicles: an in-depth review on distribution, uptake and toxicological effects in occupational and living environment. Sci Total Environ 823:153787. https://doi.org/10.1016/j.scitotenv.2022.153787

Abdillah SF, Wang YF (2023) Ambient ultrafine particle ($PM_{0.1}$): sources, characteristics, measurements and exposure implications on human health. Environ Res 218:115061. https://doi.org/10.1016/j.envres.2022.115061

Akhbarizadeh R, Dobaradaran S, Torkmahalleh MA, Saeedi R, Aibaghi R, Ghasemi F (2021) Suspended fine particulate matter ($PM_{2.5}$), microplastics (MPs), and polycyclic aromatic hydrocarbons (PAHs) in air: their possible relationships and health implications. Environ Res 192:110339. https://doi.org/10.1016/j.envres.2020.110339

Alderton D (2021) X-Ray diffraction (XRD). Encycl Geol 520–531. https://doi.org/10.1016/b978-0-08-102908-4.00178-8

Alencar W, Da Silva JAP, De Oliveira F, Ghosh A, Vasconcelos DFP, Da Silva JAP, De Freitas CM, De Moura T, Rufino F, Freire P (2022) Vibrational spectroscopy, X-ray diffraction and EDS applied to reveal the fossilization pathways of fossil shells from the Jandaíra Formation, Upper Cretaceous Northeast Brazil. Vib Spectrosc 123:103430. https://doi.org/10.1016/j.vibspec.2022.103430

ARL (NOAA Air Resources Laboratory) (2023) Real-time Environmental Applications and Display sYstem. https://www.ready.noaa.gov/index.php. (Accessed 27 November 2023)

Balch WM, Mitchell C (2023) Remote sensing algorithms for particulate inorganic carbon (PIC) and the global cycle of PIC. Earth-Sci Rev 239:104363. https://doi.org/10.1016/j.earscirev.2023.104363

Ballikaya P, Marshall J, Cherubini P (2022) Can tree-ring chemistry be used to monitor atmospheric nanoparticle contamination over time? Atmos Environ 268:118781. https://doi.org/10.1016/j.atmosenv.2021.118781

Bartholdi JJ, Goldsman P (2004) The vertex-adjacency dual of a triangulated irregular network has a Hamiltonian cycle. Oper Res Lett 32(4):304–308. https://doi.org/10.1016/j.orl.2003.11.005

Batool F, Hennig C (2021) Clustering with the average silhouette width. Comput Stat Data Anal 158:107190. https://doi.org/10.1016/j.csda.2021.107190

Bodah BW, Neckel A, Maculan LS, Milanes CB, Korcelski C, Ramírez O, Mendez-Espinosa JF, Bodah ET, Oliveira ML (2022) Sentinel-5P TROPOMI satellite application for NO2 and CO studies aiming at environmental valuation. J Clean Prod 357:131960. https://doi.org/10.1016/j.jclepro.2022.131960

Borrego C, Monteiro A, Ferreira J, Moraes M, Carvalho A, Ribeiro I, Miranda A, Moreira D (2010) Modelling the photochemical pollution over the metropolitan area of Porto Alegre, Brazil. Atmos Environ 44(3):370–380. https://doi.org/10.1016/j.atmosenv.2009.10.027

Brunner N, Mayrpeter G, Kühleitner M (2022) Parameter estimation of the Solow-Swan fundamental differential equation. Heliyon 8(10):e10816. https://doi.org/10.1016/j.heliyon.2022.e10816

Cappelletti D, Petroselli C, Mateos D, Herreras M, Ferrero L, Losi N, Gregorič A, Frangipani C, La Porta G, Lonardi M, Chernov D, Dekhtyareva A (2022) Vertical profiles of black carbon and nanoparticles pollutants measured by a tethered balloon in Longyearbyen (Svalbard islands). Atmos Environ 290:119373. https://doi.org/10.1016/j.atmosenv.2022.119373

Che W, Zhang Y, Lin C, Fung YH, Fung JCH, Lau AK (2022) Impacts of pollution heterogeneity on population exposure in dense urban areas using ultra-fine resolution air quality data. J Environ Sci 125:513–523. https://doi.org/10.1016/j.jes.2022.02.041

Dal Moro L, Maculan LS, Neckel A, De Vargas Mores G, Pivoto D, Bodah ET, Bodah BW, Oliveira ML (2021) Geotechnologies applied to the analysis of buildings involved in the production of poultry and swine to the integrated food safety system and environment. J Environ Chem Eng 9(6):106475. https://doi.org/10.1016/j.jece.2021.106475

ESA (European Space Agency) (2023a) SENTINEL-3 OLCI introduction. https://sentinels.copernicus.eu/fr/web/sentinel/user-guides/sentinel-3-olci. (Accessed 28 January 2023)

ESA (European Space Agency) (2023b) SENTINEL-3 OLCI Resolutions. https://sentinels.copernicus.eu/fr/web/sentinel/user-guides/sentinel-3-olci/resolutions. (Accessed 29 January 2023)

ESA (European Space Agency) (2023c) SENTINEL-3 OLCI Level-2 Water Product Type. https://sentinels.copernicus.eu/fr/web/sentinel/user-guides/sentinel-3-olci/product-types/level-2-water. (Accessed 30 January 2023)

Guleria RP, Chand K (2020) Emerging patterns in global and regional aerosol characteristics: a study based on satellite remote sensors. J Atmos Sol-Terr Phys 197:105177. https://doi.org/10.1016/j.jastp.2019.105177

Hamdan AM, Lubis SS, Nazla CT, Jaswita D, Maulida Z, Munandar A, Hamdi H, Ardiansyah R, Khairuzzaman H (2023) Magnetic susceptibilities of suspended sediment and microplastic abundance in a tropical volcanic estuary. Reg Stud Mar Sci 61:102927. https://doi.org/10.1016/j.rsma.2023.102927

Herrera LK, Videla HA (2009) Surface analysis and materials characterization for the study of biodeterioration and weathering effects on cultural property. Int Biodeterior 63(7):813–822. https://doi.org/10.1016/j.ibiod.2009.05.002

Huaji Z, Bai J, Wang Y, Ren J, Yang X, Jiao L (2023) Deep radio signal clustering with interpretability analysis based on saliency map. Digit Commun Netw 19:1–16. https://doi.org/10.1016/j.dcan.2023.01.010

IBGE. Brazilian Institute of Geography and Statistics (2023) Cities and states of Brazil. Demographic Data. https://cidades.ibge.gov.br/. (Accessed 1 March 2023)

INMET. National Institute of Meteorology (2023) Annual historical data. https://portal.inmet.gov.br/dadoshistoricos. (Accessed 15 March 2023)

INPE. Center for Weather Forecasting and Climate Studies (2022) Monthly and seasonal evolution of rain. In: <http://clima1.cptec.inpe.br/evolucao/pt>. (Accessed 26 March 2022)

Jia H, Wang G, Tang W, Song D, Wang X, Hong J, Zhang Z (2020) An optimized approach using cryofixation for high-resolution 3D analysis by FIB-SEM. J Struct Biol 212(1):107600. https://doi.org/10.1016/j.jsb.2020.107600

Kariyam N, Abdurakhman N, Effendie AR (2023) A medoid-based deviation ratio index to determine the number of clusters in a dataset. MethodsX 102084. https://doi.org/10.1016/j.mex.2023.102084

Ketzel M, Frohn LM, Christensen JH, Brandt J, Massling A, Andersen CT, Im U, Jensen SS, Khan J, Nielsen O, Plejdrup MS, Manders A, Van Der Gon HD, Kumar PS, Raaschou-Nielsen O (2021)

Modelling ultrafine particle number concentrations at address resolution in Denmark from 1979 to 2018 - Part 2: Local and street scale modelling and evaluation. Atmos Environ 264:118633. https://doi.org/10.1016/j.atmosenv.2021.118633

Kumar P, Skouloudis AN, Bell M, Viana M, Carotta MC, Biskos G, Morawska L (2016) Real-time sensors for indoor air monitoring and challenges ahead in deploying them to urban buildings. Sci Total Environ 560–561:150–159. https://doi.org/10.1016/j.scitotenv.2016.04.032

Kumar P, Zavala-Reyes JC, Kalaiarasan G, Abubakar-Waziri H, Young G, Mudway I, Dilliway C, Lakhdar R, Mumby S, Kłosowski M, Pain C, Adcock IM, Watson JS, Sephton MA, Chung KF, Porter AE (2022) Characteristics of fine and ultrafine aerosols in the London underground. Sci Total Environ 858:159315. https://doi.org/10.1016/j.scitotenv.2022.159315

Leong W, Kelani R, Ahmad Z (2020) Prediction of air pollution index (API) using support vector machine (SVM). J Environ Chem Eng 8(3):103208. https://doi.org/10.1016/j.jece.2019.103208

Li W (2023) The effect of China's driving restrictions on air pollution: the role of a policy announcement without a stated expiration. Resour Energy Econ 72:101360. https://doi.org/10.1016/j.reseneeco.2023.101360

Li H, Yang Z, Yan W (2022) An improved AIC onset-time picking method based on regression convolutional neural network. Mech Syst Signal Process 171:108867. https://doi.org/10.1016/j.ymssp.2022.108867

Liang Y, Gui K, Che H, Li L, Zheng Y, Zhang X, Zhang X, Zhang P, Zhang X (2023) Changes in aerosol loading before, during and after the COVID-19 pandemic outbreak in China: effects of anthropogenic and natural aerosol. Sci Total Environ 857:159435. https://doi.org/10.1016/j.scitotenv.2022.159435

Lu S, Hao X, Liu D, Wang Q, Zhang W, Liu P, Zhang R, Yu S, Pan R, Wu M, Yonemochi S, Wang Q (2016) Mineralogical characterization of ambient fine/ultrafine particles emitted from Xuanwei C1 coal combustion. Atmos Res 169:17–23. https://doi.org/10.1016/j.atmosres.2015.09.020

Mandal J, Patel PP (2021) Gauging the effects of the COVID-19 pandemic lockdowns on atmospheric pollution content in select countries. Remote Sens Appl: Soc Environ 23:100551. https://doi.org/10.1016/j.rsase.2021.100551

Marcella S, Apicella B, Secondo A, Palestra F, Opromolla G, Ciardi R, Tedeschi V, Ferrara AL, Apicella B, Galdiero MR, Cristinziano L, Modestino L, Spadaro G, Fiorelli A, Loffredo S (2022) Size-based effects of anthropogenic ultrafine particles on activation of human lung macrophages. Environ Int 166:107395. https://doi.org/10.1016/j.envint.2022.107395

Marmett B, Pires Dorneles G, Böek Carvalho R, Peres A, Roosevelt Torres Romão P, BarcosNunes R, Ramos Rhoden C (2021) Air pollution concentration and period of the day modulates inhalation of $PM_{2.5}$ during moderate - and high-intensity interval exercise. Environ Res 194:110528. https://doi.org/10.1016/j.envres.2020.110528

Maroni D, Cardoso GT, Neckel A, Maculan LS, Oliveira MLS, Bodah ET, Bodah BW, Santosh M (2021) Land surface temperature and vegetation index as a proxy to microclimate. J Environ Chem Eng 9(4):105796. https://doi.org/10.1016/j.jece.2021.105796

Martinello KD, Hower JC, Pinto DCGA, Schnorr CE, Dotto GL, Ramos CG (2022) Artisanal ceramic factories using wood combustion: a nanoparticles and human health study. Geosci Front 13(1):101151. https://doi.org/10.1016/j.gsf.2021.101151

Mehrjou A, Hosseini R, Araabi BN (2016) Improved Bayesian information criterion for mixture model selection. Pattern Recognit Lett 69:22–27. https://doi.org/10.1016/j.patrec.2015.10.004

Morillas H, Marcaida I, Maguregui M, Upasen S, Gallego-Cartagena E, Madariaga JM (2019) Identification of metals and metalloids as hazardous elements in $PM_{2.5}$ and PM_{10} collected in a coastal environment affected by diffuse contamination. J Clean Prod 226:369–378. https://doi.org/10.1016/j.jclepro.2019.04.063

Naghizadeh A, Metaxas DN (2020) Condensed silhouette: an optimized filtering process for cluster selection in K-means. Procedia Comput Sci 176:205–214. https://doi.org/10.1016/j.procs.2020.08.022

Neckel A, Oliveira ML, Maculan LS, Bodah BW, Gonçalves AC, Silva LF (2023) Air pollution in central European capital (Budapest) via self-made passive samplers and Sentinel-3B SYN satellite images. Urban Clim 47:101384. https://doi.org/10.1016/j.uclim.2022.101384

Novo R, Marocco P, Giorgi G, Lanzini A, Santarelli M, Mattiazzo G (2022) Planning the decarbonisation of energy systems: the importance of applying time series clustering to long-term models. Energy Convers Manag: X 15:100274. https://doi.org/10.1016/j.ecmx.2022.100274

Oliveira ML, Neckel A, Pinto DCGA, Maculan LS, Zanchett MRD, Silva LF (2021) Air pollutants and their degradation of a historic building in the largest metropolitan area in Latin America. Chemosphere 277:130286. https://doi.org/10.1016/j.chemosphere.2021.130286

Peng C, Deng C, Lei T, Zheng J, Zhao J, Wang D, Wu Z, Wang L, Chen Y, Liu M, Jiang J, Ye A, Ge M, Wang W (2023) Measurement of atmospheric nanoparticles: bridging the gap between gas-phase molecules and larger particles. J Environ Sci 123:183–202. https://doi.org/10.1016/j.jes.2022.03.006

Perrotti TC, De Freitas NC, Alzamora M, Sanchez DR, Carvalho NM (2019) Green iron nanoparticles supported on amino-functionalized silica for removal of the dye methyl orange. J Environ Chem Eng 7(4):103237. https://doi.org/10.1016/j.jece.2019.103237

Pryshchepa O, Buszewski B (2020) Silver nanoparticles: synthesis, investigation techniques, and properties. Adv Colloid Interface Sci 284:102246. https://doi.org/10.1016/j.cis.2020.102246

Putra YC, Wijayanto AW, Chulafak GA (2022) Oil palm trees detection and counting on Microsoft Bing Maps Very High Resolution (VHR) satellite imagery and Unmanned Aerial Vehicles (UAV) data using image processing thresholding approach. Ecol Inform 72:101878. https://doi.org/10.1016/j.ecoinf.2022.101878

Quevedo CP, Jiménez-Millán J, Cifuentes GR, Jiménez-Espinosa R (2020) Clay mineral transformations in anthropic organic matter-rich sediments under saline water environment. Effect on the detrital mineral assemblages in the Upper Chicamocha River Basin. Colombia. Appl Clay Sci 196:105776. https://doi.org/10.1016/j.clay.2020.105776

Qv H, Ma T, Tong X, Huang X, Ma Z, Feng J (2022) Clustering by centroid drift and boundary shrinkage. Pattern Recognit 129:108745. https://doi.org/10.1016/j.patcog.2022.108745

Racoviteanu A, Manley WF, Arnaud Y, Williams M (2007) Evaluating digital elevation models for glaciologic applications: an example from Nevado Coropuna, Peruvian Andes. Glob Planet Chang 59(1–4):110–125. https://doi.org/10.1016/j.gloplacha.2006.11.036

Rohra H, Pipal AS, Satsangi P, Taneja A (2022) Revisiting the atmospheric particles: connecting lines and changing paradigms. Sci Total Environ 841:156676. https://doi.org/10.1016/j.scitotenv.2022.156676

Romanovski V, Zhang L, Su X, Smorokov A, Kamarou M (2022) Gypsum and high quality binders derived from water treatment sediments and spent sulfuric acid: chemical engineering and environmental aspects. Chem Eng Res Des 184:224–232. https://doi.org/10.1016/j.cherd.2022.06.008

Saikia BK, Saikia J, Rabha S, Finkelman RB (2017) Ambient nanoparticles/nanominerals and hazardous elements from coal combustion activity: implications on energy challenges and health hazards. Geosci Front 9(3):863–875. https://doi.org/10.1016/j.gsf.2017.11.013

Sánchez-Zapero J, Camacho F, Martinez-Sanchez E, Gorroño J, León-Tavares J, Benhadj I, Tote C, Swinnen E, Muñoz-Sabater J (2023) Global estimates of surface albedo from Sentinel-3 OLCI and SLSTR data for Copernicus Climate Change Service: algorithm and preliminary validation. Remote Sens EnviroN 287:113460. https://doi.org/10.1016/j.rse.2023.113460

SDE (Department of Economic Development) (2023) Numbers of opening and extinction of companies in RS, Brazil. https://jucisrs.rs.gov.br/numeros-de-abertura-e-extincao-de-empresas-no-rs. (Accessed 15 January 2023)

Silva LF, Oliveira ML, Neckel A, Maculan LS, Batista CM, Bodah BW, Cambrussi LP, Dotto GL (2022) Effects of atmospheric pollutants on human health and deterioration of medieval historical architecture (North Africa, Tunisia). Urban Clim 41:101046. https://doi.org/10.1016/j.uclim.2021.101046

Sjövall P, Bake KD, Pomerantz AE, Lu X, Mitra-Kirtley S, Mullins OC (2021) Analysis of kerogens and model compounds by time-of-flight secondary ion mass spectrometry (TOF-SIMS). Fuel 286:119373. https://doi.org/10.1016/j.fuel.2020.119373

Tang Y, Hu S, Wang H (2020) Using P-Cl inorganic ultrafine aerosol particles to prevent spontaneous combustion of low-rank coal in an underground coal mine. Fire Saf J 115:103140. https://doi.org/10.1016/j.firesaf.2020.103140

Teixeira C, Fernandes CR, Ahern J (2022) Adaptive planting design and management framework for urban climate change adaptation and mitigation. Urban for Urban Green 70:127548. https://doi.org/10.1016/j.ufug.2022.127548

Tian X, Zhang H, Hu C, Yan Y (2023) Preparation of microfiber composite nitrogen doped carbon nanotube membranes and their degradation properties of phenol in the structured fixed bed. J Environ Chem Eng 11(1):109255. https://doi.org/10.1016/j.jece.2022.109255

Trejos EM, Silva LF, Hower JC, Flores EM, González C, Pachon JE, Aristizábal BH (2021) Volcanic emissions and atmospheric pollution: a study of nanoparticles. Geosci Front 12(2):746–755. https://doi.org/10.1016/j.gsf.2020.08.013

Vithanage M, Bandara P, Novo LAB, Kumar A, Ambade B, Naveendrakumar G, Ranagalage M, Magana-Arachchi D (2022) Deposition of trace metals associated with atmospheric particulate matter: environmental fate and health risk assessment. Chemosphere 303:135051. https://doi.org/10.1016/j.chemosphere.2022.135051

Vouitsis I, Portugal J, Kontses A, Karlsson HL, Faria M, Elihn K, Juárez-Facio AT, Amato F, Piña B, Samaras Z (2023) Transport-related airborne nanoparticles: sources, different aerosol modes, and their toxicity. Atmos Environ 301:119698. https://doi.org/10.1016/j.atmosenv.2023.119698

Wölk F, Yuan T, Kis-Katos K, Fu X (2023) A temporal–spatial analysis on the socioeconomic development of rural villages in Thailand and Vietnam based on satellite image data. Comput Commun 203:146–162. https://doi.org/10.1016/j.comcom.2023.02.017

Xu XP, Ni S, Fu M, Xin Z, Luo N, Weng W (2017) Numerical investigation of airflow, heat transfer and particle deposition for oral breathing in a realistic human upper airway model. J Therm Biol 70:53–63. https://doi.org/10.1016/j.jtherbio.2017.05.003

Xu Q, Ning L, Yuan T, Wu H (2023) Application of data mining combined with power data in assessment and prevention of regional atmospheric pollution. Energy Rep 9:3397–3405. https://doi.org/10.1016/j.egyr.2023.02.016

Yuan H, Van De Moortèle B, Epicier T (2021) Accurate post-mortem alignment for Focused Ion Beam and Scanning Electron Microscopy (FIB-SEM) tomography. Ultramicroscopy 228:113265. https://doi.org/10.1016/j.ultramic.2021.113265

Zequan C, Li G, He J, Yang Z, Wang J (2022) A new parallel adaptive structural reliability analysis method based on importance sampling and K-medoids clustering. Reliab Eng Syst Safety 218:108124. https://doi.org/10.1016/j.ress.2021.108124

Zhang X, Wang H, Wang S, Liu Y, Yu W, Wang J, Xu Q, Li X (2022) Oceanic internal wave amplitude retrieval from satellite images based on a data-driven transfer learning model. Remote Sens Environ 272:112940. https://doi.org/10.1016/j.rse.2022.112940

Zhao L, Wang J, Gao HO, Xie Y, Jiang R, Hu Q, Sun Y (2017) Evaluation of particulate matter concentration in Shanghai's metro system and strategy for improvement. Transp Res d: Transp Environ 53:115–127. https://doi.org/10.1016/j.trd.2017.04.010

Zheng X, Xiong H, Gong J, Yue L (2017) A morphologically preserved multi-resolution TIN surface modeling and visualization method for virtual globes. ISPRS J Photogramm Remote Sens 129:41–54. https://doi.org/10.1016/j.isprsjprs.2017.04.013

Zhou C, Peng X, Li X, Qi K, Gao L (2023) Stable CuFeO/Kaolin-based catalytic particle electrode in 3D heterogeneous electro-Fenton system for orange G removal: synthesis, performance and mechanism. J Environ Chem Eng 11(2):109562. https://doi.org/10.1016/j.jece.2023.109562

Zhu H, Cheng T, Li X, Ye X (2022) Comparison and evaluation of multiple satellite aerosol products over China in different scenarios under a unified criterion: preparation for consistent and high-quality dataset construction. Atmos Res 279:106374. https://doi.org/10.1016/j.atmosres.2022.106374

Zhu L, Xie C, Chen L, Dai X, Zhou Y, Pan H, Tian K (2023) Transport of microplastics in the body and interaction with biological barriers, and controlling of microplastics pollution. Ecotoxicol Environ Saf 255:114818. https://doi.org/10.1016/j.ecoenv.2023.114818

Zoheir B, Emam A, El-Wahed MAA, Soliman N (2019) Gold endowment in the evolution of the Allaqi-Heiani suture, Egypt: a synthesis of geological, structural, and space-borne imagery data. Ore Geol Rev 110:102938. https://doi.org/10.1016/j.oregeorev.2019.102938

Zorzi CGC, Neckel A, Maculan LS, Cardoso GT, Moro LD, Savio AAD, Carrasco LD, Oliveira ML, Bodah ET, Bodah BW (2022) Geo-environmental parametric 3D models of SARS-CoV-2 virus circulation in hospital ventilation systems. Geosci Front 13(6):101279. https://doi.org/10.1016/j.gsf.2021.101279

Zou Z, Yang X (2022) Volatile organic compound emissions from the human body: decoupling and comparison between whole-body skin and breath emissions. Build Environ 226:109713. https://doi.org/10.1016/j.buildenv.2022.109713